Taylor & Francis
Taylor & Francis Group

ORIGINAL RESEARCH

🔓 OPEN ACCESS | Check for updates

Loss of CMTM6 promotes DNA damage-induced cellular senescence and antitumor immunity

Hanfeng Wang[a,*], Yang Fan[a,*], Weihao Chen[a,b,*], Zheng Lv[c], Shengpan Wu[a], Yundong Xuan[a,b], Chenfeng Wang[a,b], Yongliang Lu[a,b], Tao Guo[b,d], Donglai Shen[a], Fan Zhang[a], Qingbo Huang[a], Yu Gao[a], Hongzhao Li[a], Xin Ma[a], Baojun Wang[a], Yan Huang[a], and Xu Zhang[a]

[a]Senior Department of Urology, The Third Medical Center of PLA General Hospital, Beijing, China; [b]Medical School of Chinese PLA, Beijing, China; [c]School of Medicine, Nankai University, Tianjin, China; [d]Senior Department of Paediatrics, The Seventh Medical Center of PLA General Hospital, Beijing, China

ABSTRACT

Recent studies have revealed that chemokine-like factor-like MARVEL transmembrane domain-containing family member 6 (CMTM6) promotes tumor progression and modulates tumor immunity by regulating programmed death-ligand 1 stability; however, its intrinsic functions and regulatory mechanisms in clear cell renal cell carcinoma (ccRCC) remain poorly understood. Here, we show that CMTM6 is upregulated in ccRCC tissues and is strongly associated with advanced tumor grades, early metastases, and a worse prognosis. CMTM6 depletion significantly impaired the proliferation, migration, and invasion of ccRCC cells *in vitro* and in xenograft mouse models *in vivo*. In addition, targeting CMTM6 promotes anti-tumor immunity, represented by increased infiltration of CD4^{+} and CD8^{+} T cells in syngeneic graft mouse models. Further research revealed that loss of CMTM6 triggered aberrant activation of DNA damage response, resulting in micronucleus formation and G2/M checkpoint arrest, finally leading to cellular senescence with robust upregulation of numerous chemokines and cytokines. Our findings show for the first time the novel role of CMTM6 in maintaining cancer genome stability and facilitating tumor-mediated immuno-suppression, linking DNA damage signaling to the secretion of inflammatory factors. Targeting CMTM6 may improve the treatment of patients with advanced ccRCC.

Introduction

Globally, the morbidity and mortality of renal cell carcinoma (RCC) have increased slightly in recent years.[1] Due to the lack of specific biomarkers, nearly 30% of RCC patients develop metastases at the initial diagnosis.[2] Among several histologic subtypes of RCC, clear cell RCC (ccRCC) accounts for approximately 70% of RCC diagnoses.[3] The treatment landscape for RCC has been revolutionized by the introduction of immune checkpoint inhibitors. However, the patient selection that is made to increase the response to immunotherapy, and primary and acquired resistance are still major challenges to be overcome, and better biomarkers and predictive models are urgently needed.[4,5]

DNA is vulnerable to damage by exogenous and endogenous sources that are commonly counteracted by the DNA damage response (DDR). DDR is a fundamental mechanism that sustains genome stability via the activation of a network of pathways promoting transient cell-cycle arrest and subsequent DNA repair.[6] However, persistent damage exceeding the repair capacity of cells would result in a variety of consequences, including cellular senescence and subsequent inflammatory cytokine secretion, termed the senescence-associated secretory phenotype (SASP).[7] Compelling evidence has indicated that SASP could contribute to tumor suppression by enforcing recruitment of immune cells to clear damaged or oncogene-expressing cells.[8,9]

The human chemokine-like factor (CKLF)-like MARVEL transmembrane domain-containing family member 6 (CMTM6) has recently been identified as a critical regulator for the expression of programmed death-ligand 1 (PD-L1) and anti-tumor immunity.[10,11] Overexpression of CMTM6 is strongly associated with malignant features and poor prognosis in several types of cancers, and targeting CMTM6 suppresses the stem cell-like properties of cancer cells, TGF-β induced epithelial–mesenchymal transition (EMT) and cell proliferation.[12–14] Notably, recent studies have revealed that the WEE1 inhibitors, a suppressor of DDR, can downregulate the expression of CMTM6.[15] Nevertheless, whether CMTM6 is involved in DNA damage and the specific function and molecular mechanisms of CMTM6 in carcinogenesis, development, and prognosis in ccRCC are still poorly understood.

Here, we showed that CMTM6 overexpression was strongly associated with advanced tumor grade, metastases, and adverse outcomes. CMTM6 depletion impaired proliferation and motility both *in vitro* and *in vivo*. Notably, loss of CMTM6

---

increased genome instability, which led to the activation of cell cycle arrest and cellular senescence signaling with robust secretion of inflammatory factors that might contribute to anti-tumor immunity. Collectively, these findings indicate that CMTM6 may be a novel therapeutic target for improving clinical outcomes in ccRCC patients.

Material and methods

Cell culture

Human renal proximal tubular epithelial cell line HKC, human ccRCC cell lines A498, 786-O, Caki-1, and SN12-PM6, murine RCC cell line Renca, and HEK293T cells were obtained from the National Platform of Experimental Cell Resources for Sci-Tech (Beijing, China) in September 2015 and then preserved in our laboratory, which were authenticated in January 2019 using the method described earlier.[16] A498, 786-O, Caki-1, and SN12-PM6 cells were cultured and maintained in Minimum Essential Medium (MEM), RPMI 1640, McCoy's 5A, and Dulbecco's modified Eagle's medium (DMEM) (Gibco) supplemented with 10% fetal bovine serum (FBS) (Evergreen Co. Ltd., China) and 1% penicillin–streptomycin, and Renca cells were cultured in RPMI 1640 with 10% FBS, 1% penicillin–streptomycin, and 1% non-essential amino acids. Throughout this study, all cell lines were passaged fewer than 20 times. All cells were incubated at 37°C in 5% CO_2 under mycoplasma-free conditions.

Tissue samples

After obtaining approval from the Institutional Review Board of PLA General Hospital, a total of 144 ccRCC specimens and 106 adjacent normal tissue specimens were included (from January 2015 to December 2017) on previously constructed tissue microarrays in our lab. Informed consent was obtained from all patients for the use of their tissues for scientific research. All ccRCC specimens were confirmed by a genitourinary pathology specialist according to 2016 WHO Classification of Tumors of the Urinary System and Male Genital Organs,[17] and clinical staging was performed according to the eighth American Joint Committee on Cancer TNM staging system.[18]

Plasmid construction and transfection

pLKO-shCMTM6 plasmids with short hairpin RNAs (shRNAs) targeting human and murine CMTM6 were designed (Invitrogen). The corresponding double-stranded oligonucleotides were inserted into the pLKO vector digested with AgeI and EcoRI.[19] The target sequences for shCMTM6 #1 and shCMTM6 #2 for humans and mice are listed in Supplementary Table S1. Lentivirus was produced by transfection of HEK-293ET cells with packaging DNA plus lenti-pLKO vectors, and the packaging DNA, psPAX2, and pMD2-VSVG at a 4:3:1 ratio. Transfection was performed using MaxiCap reagent kits (M&C Gene Technology), as recommended by the manufacturer. The viral supernatant was collected at 48 h and

72 h, respectively, after transfection, filtered through a 0.45 μm filter and added to target cells in the presence of polybrene (2 μg/mL, Millipore). Puromycin (2 μg/mL, Sigma) was used to treat cells for two days to kill cells that had not been infected.[19]

Antibody

Rabbit anti-CMTM6 (Sigma-Aldrich; HPA026980), rabbit anti-PD-L1 (Abcam, USA; ab213524), rabbit anti-CD4 (Abcam; ab183685), rabbit anti-CD8 alpha (Abcam; ab217344), rabbit anti-CD68 (Proteintech; 28058-1-AP), rabbit anti-CD11b (Abcam; ab133357), and rabbit anti-Ki-67 (Cell Signaling Technology; #9129) were used for immunostaining.

Rabbit anti-CMTM6 (Sigma-Aldrich, HPA026980), rabbit anti-PD-L1 (Abcam; ab213524), rabbit anti-E-cadherin (Proteintech; 20874-1-AP), rabbit anti-N-cadherin (Proteintech; 22018-1-AP), rabbit anti-Snail (Proteintech; 13099-1-AP), rabbit anti-p53 (Proteintech; 10442-1-AP), rabbit anti-cyclin B1 (Proteintech; 55004-1-AP), and rabbit anti-phospho-Histone H2A.X (Cell Signaling Technology; #9718) were used for immunoblotting.

Rabbit anti-CMTM6 (Sigma-Aldrich, HPA026980), Rabbit anti-phospho-Histone H2A.X (Cell Signaling Technology; #9718) and rabbit anti-phospho-histone H3 (Cell Signaling Technology; #53348) were used for immunofluorescence.

Immunostaining

For human and murine tissue samples, immunostaining was performed as described earlier.[20] The staining intensity (negative = 0, weak = 1, moderate = 2, strong = 3) and the proportion of stained cells (0% = 0, ≤25% = 1, 26%–50% = 2, 51%–75% = 3, ≥76% = 4) was assessed using the German semi-quantitative scoring system. The final score for each specimen was obtained by multiplying the intensity scores by their extent, ranging from 0 (minimum score) to 12 (maximum score). Tumor-infiltrating immune cells were assessed as described previously.[21] All intratumoral immune cells were counted in five fields at a magnification of ×200, and the average number of cells was calculated.

Immunoblotting

Cells were lysed using RIPA buffer (Thermo Scientific) supplemented with complete protease inhibitor (Roche) and phosphatase inhibitor cocktail (Thermo Scientific), followed by pelleting of insoluble material by centrifugation. Lysates were heated to 95°C in SDS sample buffer for 10 min, separated by SDS–PAGE, and transferred to PVDF membranes (Millipore). Membranes were immunoblotted with the indicated antibodies, and reactive bands were visualized using West Pico (Thermo Scientific). Stripping buffer (Solarbio) was used to strip the immunoblot for reprobing according to the manufacturer's instructions.

Immunofluorescence

Cells seeded on glass slides were prepared. Fixation was performed with 4% paraformaldehyde for 10 min at room temperature, followed by permeabilization with 0.3% Triton

X-100/PBS for 10 min on ice. Goat serum (5%) was used for blocking. Cells were incubated at 4°C overnight with primary antibodies and at room temperature for 1 h with Alexa Fluor 488 or 594 conjugated secondary antibodies successively; nuclei were stained with 0.2 mg/mL DAPI. Imaging was performed on a TissueFAXS (TissueGnostics GmbH, Vienna Austria) with a Zeiss Axio Imager Z2 Microscope System at 20× magnification and DeltaVision Restoration Microscope (General Electric Company, USA) with a 60×/NA 1.42 oil immersion objective (Olympus, Japan).[19] Volocity software (version 6.0) was used to analyze the images.

5-ethynyl-2'-deoxyuridine (EdU) staining

EdU staining was performed using EdU Imaging Kits (Cy3) (APExBIO) according to the manufacturer's protocol. Cells seeded on glass slides were prepared and exposed to a range of EdU concentrations (5, 10, and 20 μM) for 2 h at 37°C. Further, the cells were fixed with 4% paraformaldehyde for 15 min and permeabilized with 0.5% Triton X-100/PBS for 20 min at room temperature. For the EdU click reaction, the cells were treated with staining solution for 30 min at room temperature in the dark. Nuclei were stained with 0.2 mg/mL DAPI.

Real-time PCR

Total RNA extraction from cells was performed by using the PARIS™ Kit (Applied Biosystems) according to the manufacturer's protocol, which was then reverse-transcribed to obtain cDNA using TransScript First-Strand cDNA Synthesis SuperMix (TransGen Biotech). Real-time PCR was performed using an Applied Biosystems 7500 Detection system using Maxima SYBR Green/ROX qPCR Master Mix Assays (TransGen Biotech). The relative quantification of mRNA was normalized to human peptidylprolyl isomerase A (PPIA) and then calculated using the $2^{-\Delta\Delta C_T}$ method.[22] Primer sequences that were used in real-time PCR are listed in Supplementary Table S2.

Cell proliferation assay

Cells were seeded onto a 6-well plate and cultured for 48 h, 60 h, and 72 h respectively, and the proliferation index for cells was calculated and plotted.

Wound healing assay

Cells were seeded onto 6-well plates. Confluent monolayer cells were scraped with a plastic 200 μL pipette tip and then washed with PBS three times to remove cell debris and suspension cells. The wound closure was photographed at different time points (0, 6, and 12 h) after scraping. Under 100× magnification, the coverage of the scraping area was measured by considering viable cells migrating from both sides.

Migration and invasion assay

Cells were seeded in transwell chambers with an 8 μm pore polyethylene terephthalate filter membrane (Corning). The chamber membranes were coated with 20 μL Matrigel (Corning) before cell seeding for the invasion assay. After incubation, the chamber membranes were fixed with 4% paraformaldehyde and stained with 1% crystal violet, and the cells on the upper side of the chamber membranes were removed. The number of cells that invaded through the membrane was visually counted in five random microscopic fields (100× magnification).

Cell cycle synchronization

Cells were seeded on 6-well plates. Negative control group (NC): cells were cultured with 10% FBS regular medium for 24 h; G0 group: cells were cultured with FBS-free medium for 24 h; G1/S group: thymidine (250×) was added into the 10% FBS regular medium for 24 h (2 mM final concentration); G2/M group: Synchronize cells at G1/S phases with treatment of thymidine block procedure, and then release cells form thymidine block to grow for 4 h, added nocodazole into 10% FBS regular medium to a final concentration of 100 nM for 8 h, collect the mitotic cells by mechanical shake-off.[23]

Flow cytometry

A DNA labeling solution (Cytognos) was used. Cells were collected and washed with pre-cold PBS and then fixed in 75% ethanol at 4°C overnight. The fixed cells were rewashed with PBS, and RNase A and propidium iodide (PI) were added sequentially to stain the cells according to the manufacturer's protocol. Cells were analyzed using a FACS-Calibur flow cytometer (BD Biosciences), and the data were analyzed using Cell Quest Pro software (BD Biosciences).

Senescence assay

Cells were seeded on 6-well plates. Senescence staining was performed using a Senescence β-Galactosidase (SA-β-Gal) Staining Kit (Beyotime) according to the manufacturer's instructions.

Mouse orthotopic syngeneic graft and xenograft renal cancer model

Animal studies were approved and conducted under the oversight of the Institutional Animal Care and Use Committee of the PLA General Hospital. Cells (1×10^6) suspended in PBS/Matrigel (Corning) were implanted into the right kidneys of 4–5 week old male BALB/c nude mice for xenograft model and BALB/c mice (Vital River, Beijing) for syngeneic graft (8 mice per group). All mice were sacrificed after 3 weeks and the lesions, including the orthotopic syngeneic graft, xenograft tumors, and lung metastatic nodules, were measured (in vivo bioluminescent imaging for xenograft model).

EILSA

ELISA assay was performed to measure the serum concentrations of Ccl2, Cxcl8 and Tnf-α ELISA Kits (MEIMIAN) in mouse orthotopic syngeneic graft models according to the manufacturer's instructions.

Statistical analyses

Data are presented as the mean ± SEM from at least three independent experiments. Student's *t*-test, the Mann–Whitney *U* test, or ANOVA test was applied for comparisons, as appropriate. The Kaplan–Meier method was used to analyze survival, and the log-rank test was used to evaluate differences in survival. Independent prognostic factors were identified using multivariate Cox proportional hazards models. All statistical analyses were performed using SPSS (version 22.0; SPSS Inc., USA). The level of significance was set at $*p < .05$, $**p < .01$, and $***p < .001$.

Results

CMTM6 expression is upregulated in ccRCC and associated with poor outcomes

To explore the protein expression profile of CMTM6 and its potential clinical role in ccRCC, we first performed Western blotting for 10 pairs of ccRCC tissues and corresponding adjacent normal tissues. The data showed that CMTM6 was significantly elevated in nine ccRCC tissues compared to that in adjacent normal tissues (Figure 1a). Subsequently, a tissue microarray including 144 ccRCC samples and 106 normal tissues was used for validation by immunohistochemistry (IHC). Consistently, the histoscore of CMTM6 in ccRCC tissues was markedly higher than that in normal tissues (Figure 1b). However, we detected the expression of PD-L1 in the same tissue microarray and found no correlation between the expression of CMTM6 and PD-L1 in ccRCC tissues (Supplementary Fig. S1A, S1B). According to the status of tumor grade, four subgroups were made, and quantitative analyses indicated that the expression level of CMTM6 significantly increased along with the ascending tumor grade. Specifically, the expression of CMTM6 was significantly higher in advanced tumor grades (III and IV) than in low tumor grades (I and II) (Figure 1c). Moreover, IHC demonstrated that CMTM6 protein was remarkably upregulated in ccRCC patients with preoperative distant metastases (Figure 1d) and lymph node metastases (Figure 1e).

We next assessed the association between CMTM6 expression and prognosis in ccRCC patients who were enrolled in the study and whose tissue specimens were used in the tissue microarray. These patients were divided into two groups based on the cutoff value of the CMTM6 histoscore, which was determined by receiver operating curve analysis. Samples with histoscores of ≤ 6 and > 6 were assigned to the CMTM6-low and CMTM6-high groups, respectively. Kaplan–Meier analysis showed that patients with high CMTM6 levels had worse overall survival (OS) than those with low CMTM6 levels (log-rank test $p = .0001$, figure 1f). Clinicopathological parameters with $p < .05$ screened using univariate Cox analysis were

included in multivariate analyses, and the result demonstrated that age [hazard ratio (HR) = 1.047, 95% confidence interval (95% CI) = 1.011–1.085, $p = .009$], CMTM6 expression [HR = 1.143, 95% CI = 1.048–1.246, $p = .002$], and distant metastasis [HR = 2.591, 95% CI = 1.297–4.889, $p = .006$] were independent risk factors for progression-free survival (PFS) for patients with ccRCC after surgery; simultaneously, CMTM6 expression (HR = 1.150, 95% CI = 1.042–1.269, $p = .005$), as well as distant metastasis [HR = 3.872, 95% CI = 1.866–8.034, $p < .001$] were also found to be independent risk factors for OS (Figure 1g).

CMTM6 depletion impairs the abilities of ccRCC cell proliferation, migration, and invasion

To elucidate the results derived from ccRCC tissues and the specific biological function of CMTM6 in ccRCC, we first measured the protein levels of CMTM6 and PD-L1 in normal renal epithelial cells HKC and a panel of ccRCC cell lines (A498, 786-O, Caki-1, and SN12-PM6). Among these cell lines, CMTM6 was expressed at a slight lower level in A498 cells; however, PD-L1 expression was relatively lower in Caki-1 and SN12-PM6 cells in particular on both mRNA and protein levels (Figure 2a, Supplementary Fig. S2A). 786-O and Caki-1 cell lines were used for further *in vitro* studies. Two distinct shRNAs targeting CMTM6 were generated, and the knockdown efficacy was confirmed in 786-O and Caki-1 cells after stable transduction of shRNA plasmids. However, no difference in PD-L1 expression was observed in either cell line between the shCMTM6 and negative control (NC) groups (Figure 2b). To further confirm that CMTM6 had no influence on PD-L1 expression, we treated Caki-1 cells and corresponding Caki-1-shCMTM6 cells with IFN-γ treatment. As expected, IFN-γ significantly upregulated the expression of PD-L1 even under CMTM6 depletion (Supplementary Fig. S2B). MDA-MB-231 cell, a human breast cancer cell line, was used as the positive control.[10] CMTM6 knockdown significantly decreased the expression of PD-L1 in MDA-MB-231 cells (Supplementary Fig. S2C).

The effect of CMTM6 depletion on cell proliferation was measured on the 4th day after lentivirus infection and showed remarkable inhibition of cell growth in comparison with that of control cells (Figure 2c). The wound healing assay showed that the scratching area was covered at a significantly slower speed with CMTM6 knockdown at 12 h in both 786-O and Caki-1 cells (Figure 2d). Cell migration and invasion, assessed by transwell assay with or without Matrigel coating assays, were attenuated in 786-O- and Caki-1-shCMTM6 cells, compared to those in control cells (Figure 2e). A previous study demonstrated that CMTM6 could affect the maintenance of EMT phenotypes. Therefore, we detected a series of markers related to EMT by Western blotting, including N-cadherin, E-cadherin, and Snail. As shown in figure 2f, increased expression of E-cadherin with concomitant decreased expression of N-cadherin and Snail was observed in both 786-O and Caki-1 cells after silencing CMTM6. Thus, CMTM6 might promote metastasis by enhancing EMT, and inhibition of CMTM6 could impair cell proliferation and motility.
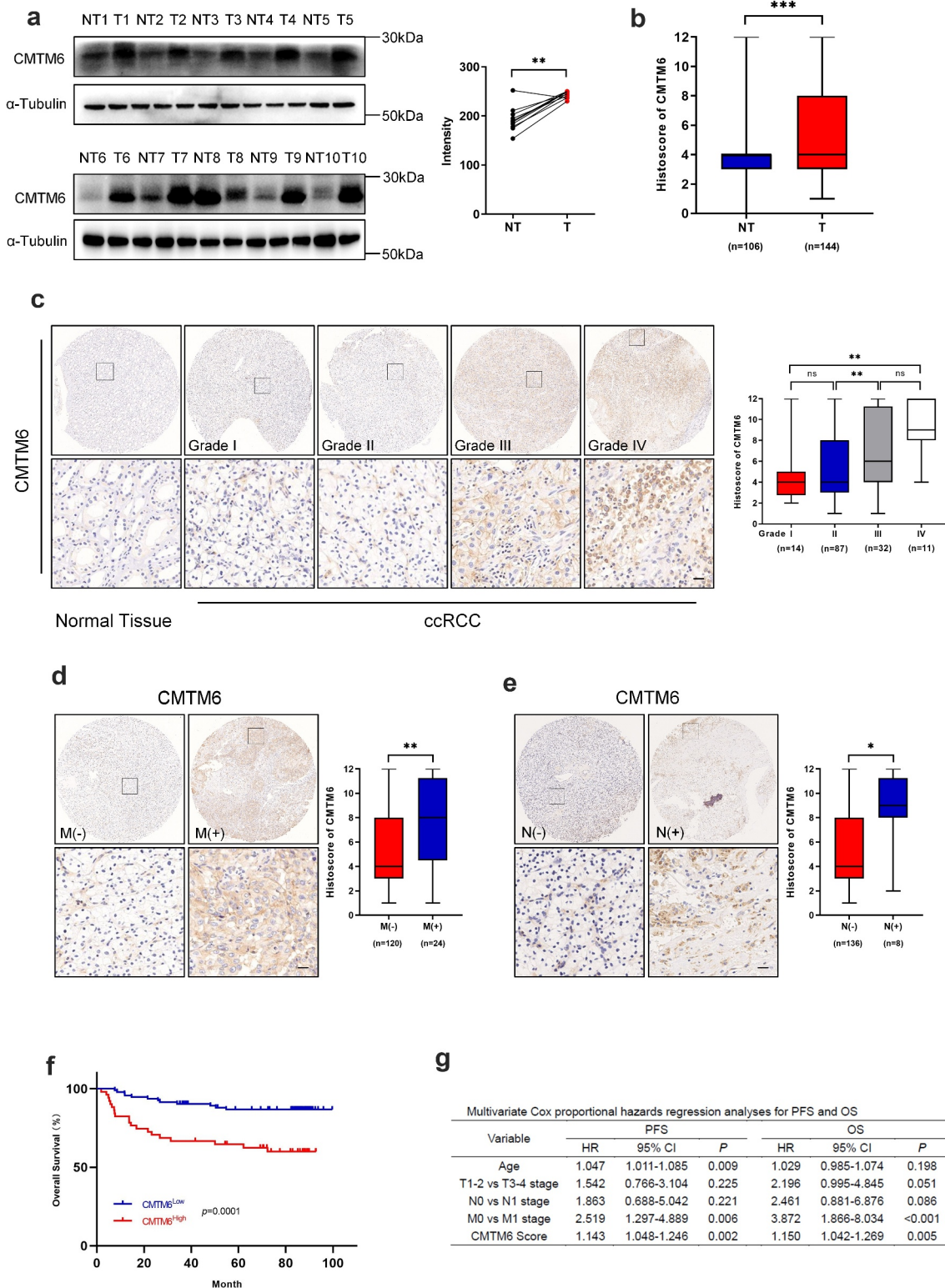
Figure 1. CMTM6 expression is upregulated in ccRCC and associated with poor outcomes. (a) Protein expression of CMTM6 in 10 pairs of ccRCC tissues (t) and corresponding adjacent normal tissues (NT) by Western blot assay, and quantitative analysis based on intensity values of bands. (b) Comparison of CMTM6 immunohistochemical (IHC) scores between ccRCC tissues (T) (n = 144) and normal tissues (NT) (n = 106) by tissue microarrays. (c) Representative IHC staining images of CMTM6 vary with tumor grades and comparison of CMTM6 IHC scores among groups with different tumor grades. The scale bar represents 20 μm. (d) Representative IHC staining images of CMTM6 in ccRCC tissues with absence or presence of preoperative distant metastases (m), and quantitative analysis between groups. The scale bar represents 20 μm. (e) Representative IHC staining images of CMTM6 in ccRCC tissues with absence or presence of preoperative lymph nodes metastases (n), and quantitative analysis between groups. The scale bar represents 20 μm. (f) Overall survival (OS) of ccRCC patients enrolled in the tissue microarray study was estimated using Kaplan–Meier analysis according to low CMTM6 expression (IHC score ≤6) or high CMTM6 expression (IHC score > 6). The p value is calculated using the log-rank test. (g) Multivariate Cox proportional hazards regression analyses for progression-free survival (PFS) and OS for ccRCC patients enrolled in the tissue microarray study. The data is represented as means ± SEM. P values are calculated using the Mann–Whitney U test (* $p < .05$, ** $p < .01$, *** $p < .001$).
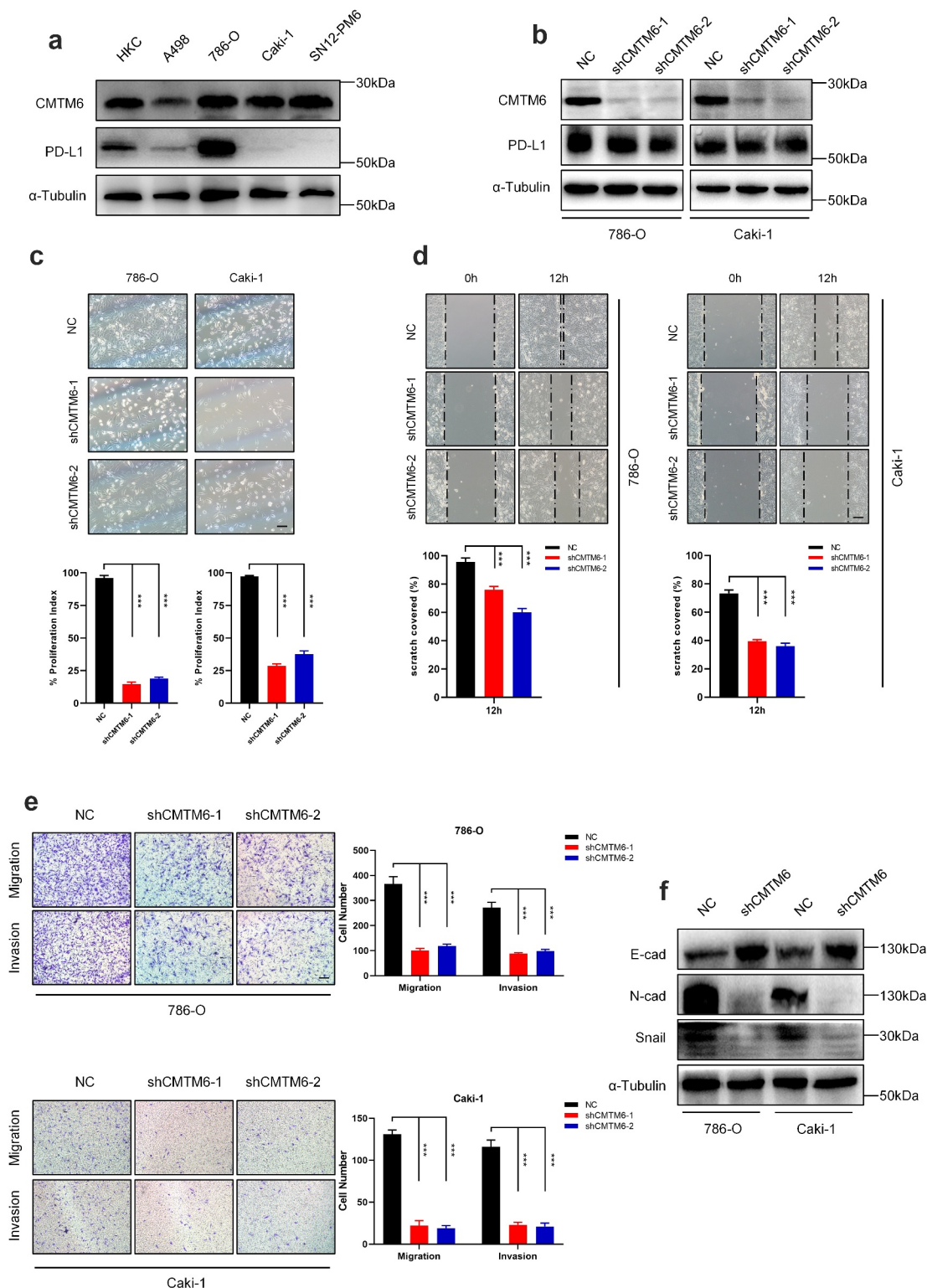
Figure 2. CMTM6 depletion impairs the abilities of ccRCC cell proliferation, migration and invasion. (a) Relative CMTM6 and corresponding PD-L1 protein levels in HKC cells and a panel of ccRCC cell lines. (b) Efficiency of CMTM6 knockdown is validated in 786-O and Caki-1 cells. (c) CMTM6 knockdown suppresses cell growth of 786-O and Caki-1 cells. The indicated cells are infected with lentiviral particles for 4 days followed by bright-field imaging (Left) and quantification (Right). The scale bar represents 100 μm. (d) Wound-healing assay indicates that CMTM6 knockdown suppresses viability of 786-O and Caki-1 cells. The scale bar represents 100 μm. (e) Transwell assay indicates impaired abilities of migration and invasion of 786-O and Caki-1 cells treat with shCMTM6. The scale bar represents 100 μm. All the functional assays above are independently repeated three times in triplicate. (f) Western blot of EMT-related genes expression in 786-O and Caki-1 cells with stably expressing control shRNA and shCMTM6. The data is represented as means ± SEM. *P*-values are calculated using the two-tailed Student's *t*-test (* $p < .05$, ** $p < .01$, *** $p < .001$).

Inhibition of CMTM6 induces G2/M checkpoint arrest and micronucleus formation via DNA damage

Deregulated cell cycle progression is a hallmark of the limitless proliferation of cancers, and targeting cyclin-dependent kinases to block cell proliferation has been verified as an effective anti-cancer therapy.[24] RNA-sequencing (RNA-seq) analysis based on Gene Ontology (GO) Biological Process indicated that the cell cycle process was significantly altered after CMTM6 depletion (Supplementary Fig. S3A). To understand the mechanisms underlying the function of CMTM6 in the cell cycle, we first measured its cellular location and fundamental expression pattern during cell cycle progression in 786-O cells. Immunofluorescence revealed that CMTM6 was not only localized in the cellular cytoplasm and membrane, but also in the nucleus (Supplementary Fig. S3B). Treatment of 786-O cells with nocodazole, an agent for synchronization for G2/M phases, revealed that CMTM6 protein and mRNA levels fluctuated during the cell cycle and were significantly elevated in the G2/M phase (Figure 3a,b). PD-L1 was used as positive control and its expression was significantly upregulated after nocodazole treatment.[24] Flow cytometry analysis revealed that CMTM6 knockdown induced a remarkable accumulation of cells in the G2/M phase in both 786-O and Caki-1 cells (Figure 3c). To further confirm the actual arrest point, we detected and quantified the cells in S anaphase and M phase by EdU staining and immunofluorescence of *p*-histone H3. The results showed that both ratios of positive cells stained with EdU and *p*-histone H3 were not significantly different between 786-O-shCMTM6 cells and control cells. Therefore, CMTM6 depletion led to G2/M checkpoint arrest (Supplementary Fig. S3C, S3D).

Simultaneously, the formation of numerous micronuclei was observed in 786-O-shCMTM6 cells by immunofluorescence staining with DAPI (Figure 3d). It has been reported that G2/M checkpoint arrest and micronucleus formation mainly result from mitotic checkpoint activation and anaphase chromosome mis-segregation, which is commonly induced by DNA damage.[25,26] To confirm the occurrence of DNA damage, we analyzed the levels of γH2A.X, a specific DNA damage marker, by immunofluorescence. We found that CMTM6 depletion significantly increased the formation of γH2A.X-positive micronucleus, the number of γH2A.X positive cells, and γH2A.X foci (Figure 3d-f). Consistently, Western blot assay showed that γH2A.X protein levels were remarkably elevated in 786-O- and Caki-1-shCMTM6 cells compared with control cells. However, CMTM6 depletion concomitantly downregulated the protein levels of p53 and cyclin B1 in both 786-O and Caki-1 cells (Figure 3g). Together, these findings indicated that CMTM6 depletion caused DNA damage following induction of G2/M checkpoint arrest and micronucleus formation.

Downregulation of CMTM6 induces cellular senescence with SASP and upregulates cell cycle-dependent inflammatory factors

To verify the biological behavior and explore other potential mechanisms involving CMTM6, we analyzed the CMTM6-dependent transcriptome in 786-O- and Caki-1-shCMTM6 cells by RNA-seq analysis. The Kyoto Encyclopedia of Genes and Genomes (KEGG) analysis of CMTM6-altered genes were enriched in multiple signaling pathways, including proliferation-related pathways, adhesion and tight junctions, and inflammatory response-related pathways, which ranked after proteasome (Supplementary Fig. S4). Collectively, these data indicate that CMTM6 plays multiple roles in the development and progression of ccRCC cells.

We further explored the RNA-seq data and found that numerous immune-related factors were involved in the top 30 altered genes that were significantly elevated after CMTM6 depletion (Figure 4a). Previous studies have showed that persistent DDR triggers cellular senescence following the development of SASP, represented by upregulation of the expression and secretion of interleukin 6 (IL6), C-X-C motif chemokine ligand 8 (CXCL8), C-C motif chemokine ligand 2 (CCL2), CCL5 and matrix metallopeptidase 9 (MMP9).[27,28] To determine whether the upregulated inflammatory cytokines were cellular senescence-mediated, we first validated the RNA-seq data, which was performed for random 10 inflammatory cytokines in new 786-O-shCMTM6 and 786-O-shNC cells. All the indicated factors were consistent with the results obtained by RNA-seq (Figure 4b). The SA-β-Gal staining also indicated that the positivity for SA-β-gal in 786-O-shCMTM6 cells was significantly higher with the transformation of cell morphology from a rounded contour to an enlarged flattened shape and vacuolization compared to that of control cells (Figure 4c). Notably, some genes were not involved in traditional SASP, such as CSF2, IL12A, and IL24. To further study whether the expression of these indicated chemokines and cytokines is associated with G2/M checkpoint arrest, we measured the fundamental expression of the selected cytokines at different cell cycle phases in 786-O cells. Except for TNF and CCL5, the other factors also fluctuated with cell cycle progression and were remarkably elevated in G2/M phases (Figure 4d). Taken together, these results indicate that elevated expression of the indicated chemokines and cytokines caused by CMTM6 depletion was not only due to SASP, but also associated with a cell cycle-dependent manner.

CMTM6 depletion suppresses xenograft tumor growth and metastasis *in vivo*

To confirm the suppression phenotype of CMTM6 depletion *in vivo*, we first established an orthotopic implantation model in BALB/c nude mice by transplanting the invasive ccRCC cell line SN12-PM6 stably expressing luciferase and control shRNA or shCMTM6 into the right subrenal capsule. The newly generated SN12-PM6-shCMTM6 cells were validated by proliferation index and Western blotting *in vitro* (Supplementary Fig. S5A, S5B). On day 21 after injection, bioluminescent imaging showed that the signals in the kidneys were significantly higher in the control group than in the shCMTM6 group (Figure 5a). All mice were then sacrificed, and the tumors were harvested. Orthotopic xenograft tumor weights of the shCMTM6 group were remarkably reduced compared to those of the control group (Figure 5b, Supplementary Fig. S5C). Histopathological analysis of tumors and lungs was performed to confirm the tumor type and the appearance of primary tumors and
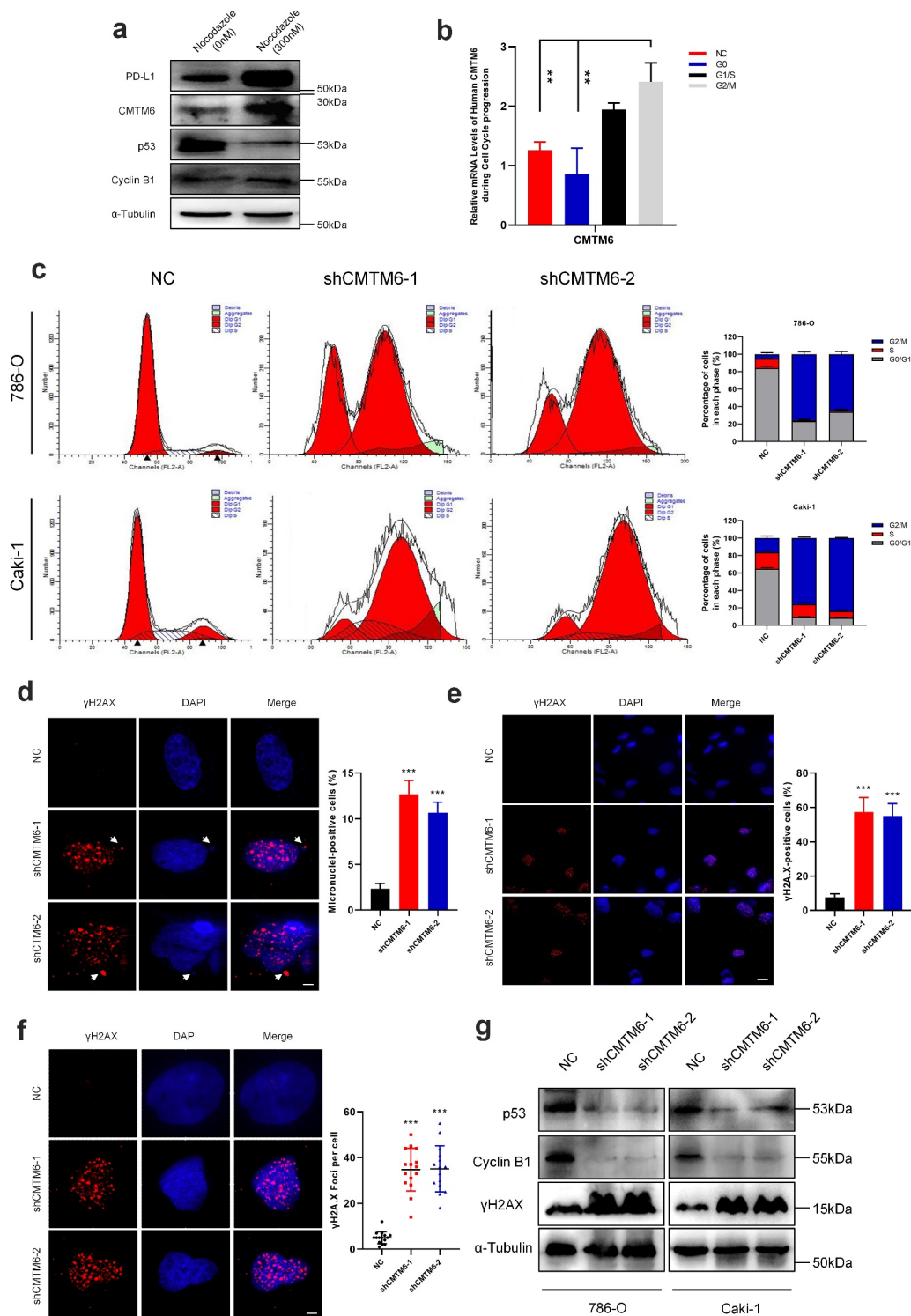
Figure 3. Inhibition of CMTM6 induces G2/M checkpoint arrest and micronucleus formation via DNA damage (a) Western blot for 786-O cells treated with indicated concentrations of nocodazole for 8 h before harvesting. (b) qRT-PCR analysis for CMTM6 mRNA levels at different phases of cell cycle in 786-O cells. (c) Flow cytometry analyses and quantitative analyses for cell cycle of 786-O and Caki-1 cells transduced with control shRNA or shCMTM6. (d) Representative immunofluorescent staining of γH2A.X-positive micronuclei (indicated by white arrows) in 786-O cells transduced with control shRNA or shCMTM6, and quantitative analysis for the number of micronucleus in each group. The scale bar represents 5 μm. (e) Representative immunofluorescent staining of γH2A.X and quantitative analysis for positive cells. The scale bar represents 20 μm. (f) Representative immunofluorescent staining of γH2A.X and quantitative analysis for the number of foci in each cell. The scale bar represents 5 μm. (g) Western blot for indicated genes expression in 786-O and Caki-1 cells transduced with control shRNA or shCMTM6. The data is represented as means ± SEM. P values are calculated using the two-tailed Student's t-test or Mann–Whitney U test (* $p < .05$, ** $p < .01$, *** $p < .001$).
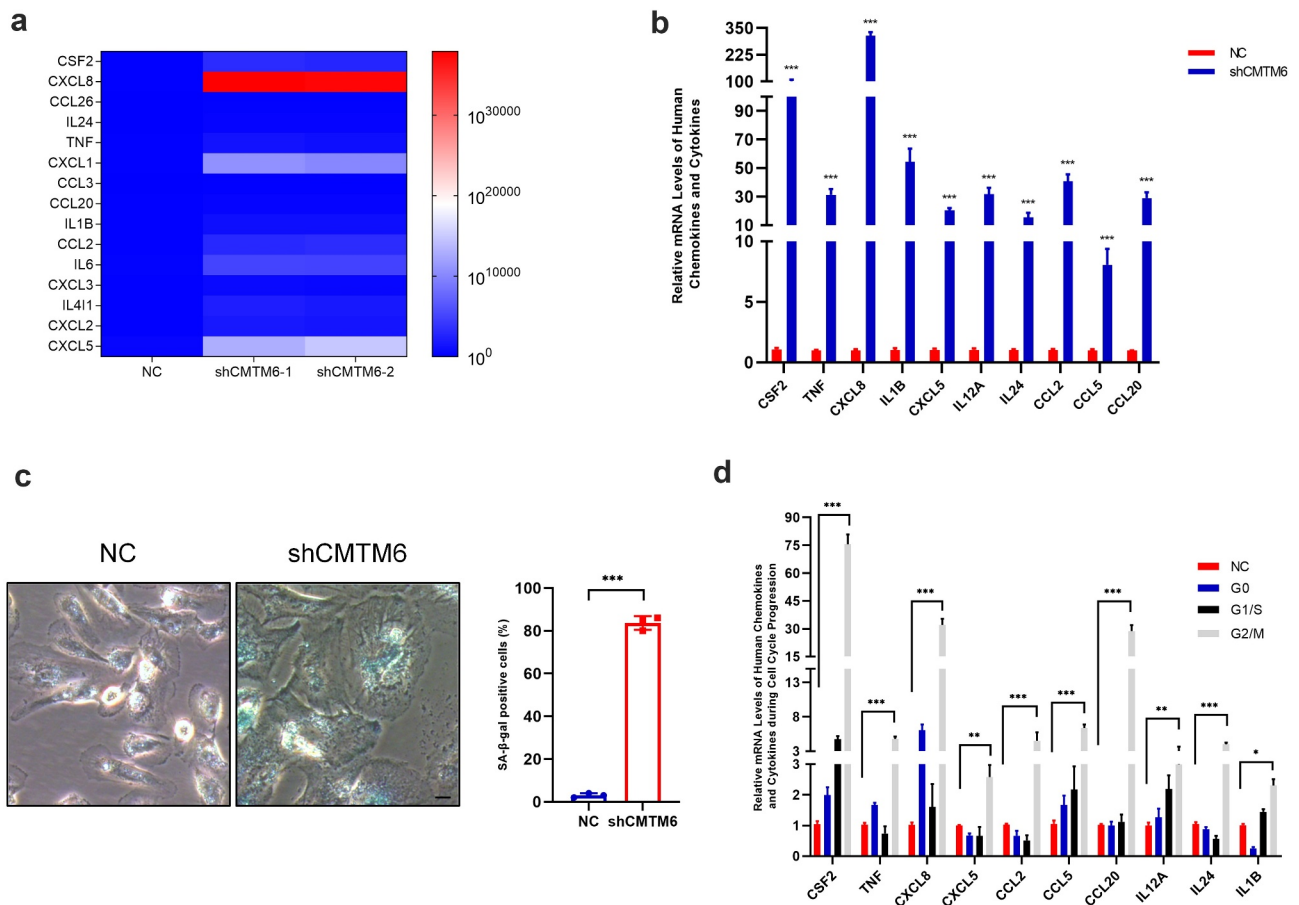
Figure 4. Downregulation of CMTM6 induces cellular senescence with SASP and upregulates cell cycle-dependent inflammatory factors. (a) Heat map of upregulated inflammatory cytokines with fold change > 5 in RNA-seq analysis for 786-O and Caki-1 cells transduced with control shRNA or shCMTM6. (b) qRT-PCR analysis for validating the difference for the indicated inflammatory cytokines in new 786-O cells transduced with control shRNA or shCMTM6. (c) SA-β-gal staining for 786-O cells transduced with control shRNA or shCMTM6, and quantitative analysis for the positive cells. The scale bar represents 50 μm. (d) qRT-PCR analysis for testing the expression of the indicated inflammatory cytokines in different phases of cell cycle. The data is represented as means ± SEM. P values are calculated using the two-tailed Student's t-test (* $p < .05$, ** $p < .01$, *** $p < .001$).

metastases (Figure 5c). To determine whether the suppressed tumor growth and metastases were due to impaired proliferation induced by CMTM6 depletion, we immunostained tumors for the targeted CMTM6, proliferation marker Ki-67, and DNA damage marker γH2A.X. Consistent with the *in vitro* results, CMTM6 knockdown was valid in tumors from nude mice in the shCMTM6 group (Figure 5d). Moreover, Ki-67 positive cells were reduced abundantly in tumors from the shCMTM6 group compared to those from the control group. In contrast, γH2A.X positive cells were significantly increased in the shCMTM6 group compared to the control group (Figure 5d,e). Together, these data indicate that targeting CMTM6 suppresses ccRCC tumor growth and metastases *in vivo*, which is consistent with our *in vitro* results.

CMTM6 silencing remodels tumor microenvironment and promotes antitumor immunity

To investigate whether CMTM6 loss promotes anti-tumor immune response to inhibit tumor growth and metastasis, we performed orthotopic syngeneic graft models by implanting Renca cells stably expressing control shRNA or shCMTM6 into the right subrenal capsule of male immunocompetent

BALB/c mice or immunodeficient BALB/c nude mice respectively. The newly generated Renca-shCMTM6 cells were validated using qRT-PCR *in vitro* (Supplementary Fig. S6A). The effect of CMTM6 depletion on cell proliferation was also measured on the 4th day after lentivirus infection and showed remarkable inhibition of cell growth in comparison with that of the control group (Supplementary Fig. S6B). qRT-PCR assay was also performed in new samples of Renca stably expressing control shRNA or shCMTM6 for measuring several chemokines and cytokines. Except for Tnf, the remaining factors were consistent with the results of RNA-seq (Supplementary Fig. S6C). Compared to control shRNA group, CMTM6 knockdown in Renca cells significantly reduced primary tumor growth both in BABL/c mice and BABL/c nude mice; quantitative analysis indicated the extent of tumor growth in BABL/c mice was much restricted than that in BABL/c nude mice (Figure 6a,b). Moreover, similar tendency was observed in lung metastasis (Figure 6c,d). These data suggested the critical role of adaptive immunity in tumor suppression. We further analyzed the tumor microenvironment alteration in BALB/c mouse models. IHC staining showed that the intratumor infiltration of CD4+ and CD8+ T cells were remarkably increased and total CD11b+ cells, commonly contain macrophages and myeloid-derived cells
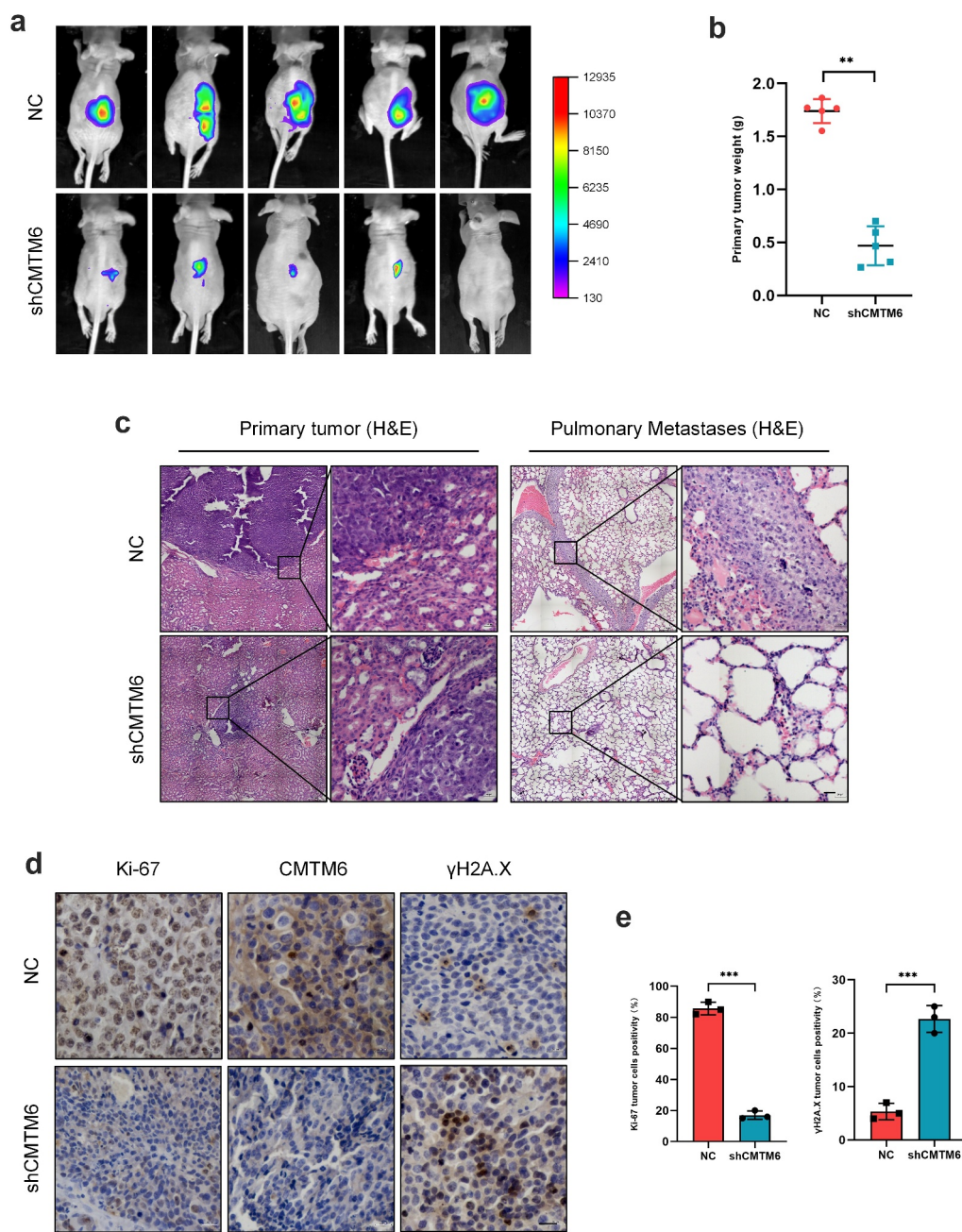
Figure 5. CMTM6 depletion suppresses xenograft tumor growth and metastasis *in vivo*. (a) Representative bioluminescent images of nude mice undergone orthotopic implantation with Luc-labeling SN12-PM6 cells stably transfected by control shRNA or shCMTM6. (b) Tumor were resected on day 21 and measured. (c) Representative H&E images of the primary tumors and lungs with metastatic lesions. Scale bar represents 20 μm. (d) Representative IHC staining images of Ki-67, CMTM6 and γH2A.X for primary renal tumors. The scale bar represents 20 μm. (e) Quantitative analyses for Ki-67 and γH2A.X positive SN12-PM6 cells stably expressing control shRNA or shCMTM6. The data is represented as means ± SEM. *P* values are calculated using the two-tailed Student's *t*-test (* $p < .05$, ** $p < .01$, *** $p < .001$).

(MDSC), were found to be significantly reduced in tumors from shCMTM6 group. However, further staining for CD68+ indicated that there was no difference in macrophage between two groups (Figure 6e). In addition, we randomly chose three chemokines and used EILSA assay to measure their serum concentrations in models. Surprisingly, the concentration of Ccl2 was significantly lower in both shCMTM6 groups in comparison with that in control shRNA group, and there was no statistically significance among groups for Cxcl8 and Tnf-α (Supplementary Fig. S6D). Consistently, Ki-67 positive cells decreased significantly in tumors from the shCMTM6 group compared to those from the control group. In contrast, γH2A.X positive cells

significantly increased in the shCMTM6 group compared to the control group (Supplementary Fig. S6E). Collectively, apart from the significant inhibition on proliferation and motility for tumor cells, loss of CMTM6 could also promote the infiltration of CD4+ and CD8+ T cells in tumors and enhance anti-tumor immunity that further contributes to tumor control.

Discussion

Growing evidence has indicated that CMTM6 has predictive value for oncological outcomes in malignancies.[29] In this regard, CMTM6 overexpression was not only highly correlated
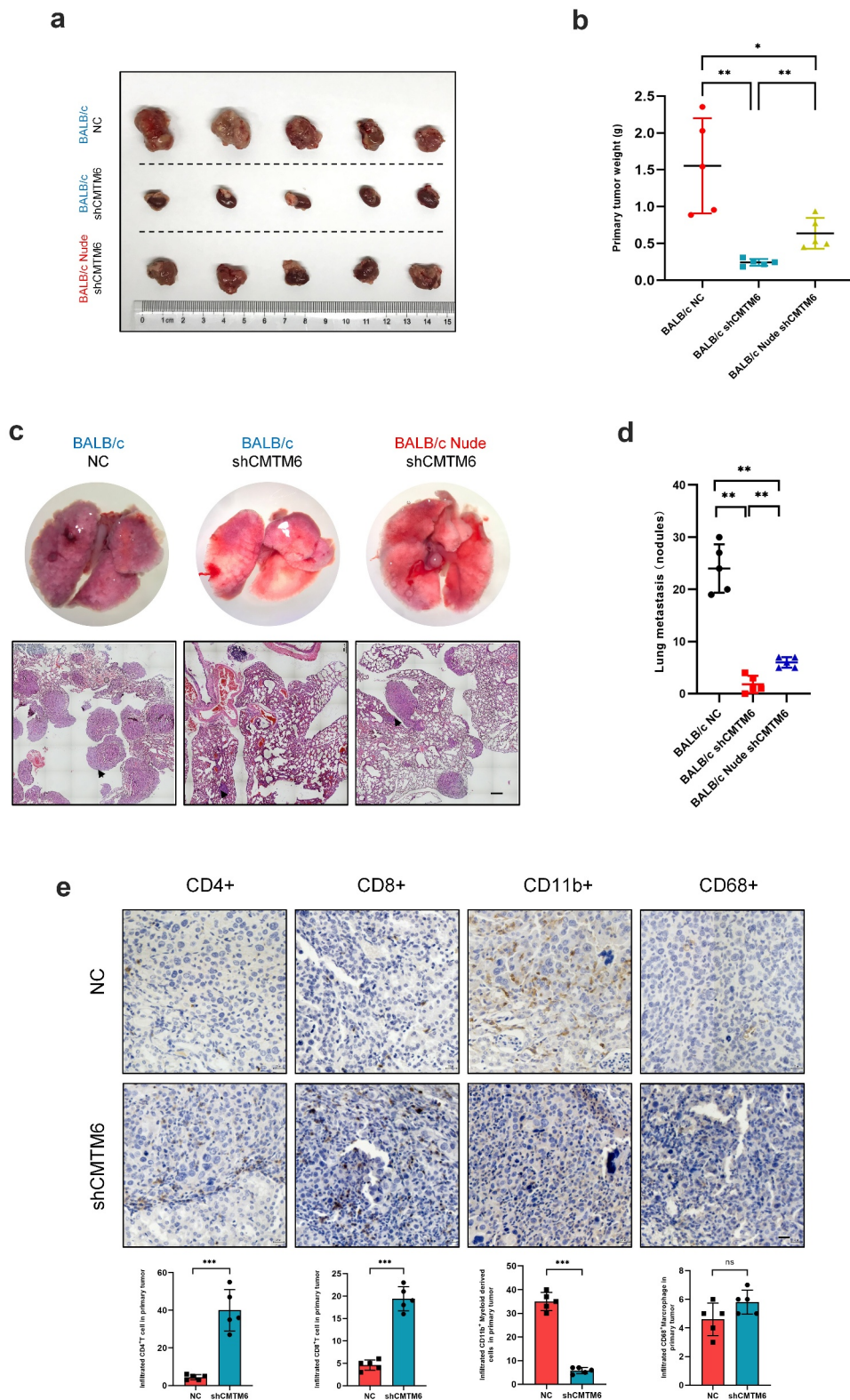
Figure 6. CMTM6 silencing remodels tumor microenvironment and promotes antitumor immunity (a) BALB/c mice and BALB/c Nude mice underwent orthotopic implantation of Renca cells stably expressing control shRNA or shCMTM6 respectively, and then tumor masses were resected on day 14. (b) Tumor weights on day 14 (n = 5). (c) Representative H&E staining images of the lungs with metastatic nodules (black arrow indicated metastatic nodules). The scale bar represents 20 μm. (d) Quantitative analysis for the amount of lung metastatic lesions. (e) Representative IHC staining images and quantitative analysis of CD4+, CD8+, CD11b+, and CD68+ in paraffin-embedded syngeneic graft tumors of BALB/c mice. The scale bar represents 20 μm. The data is represented as means ± SEM. *P* values are calculated using the two-tailed Student's *t*-test (* *p* < .05, ** *p* < .01, *** *p* < .001).
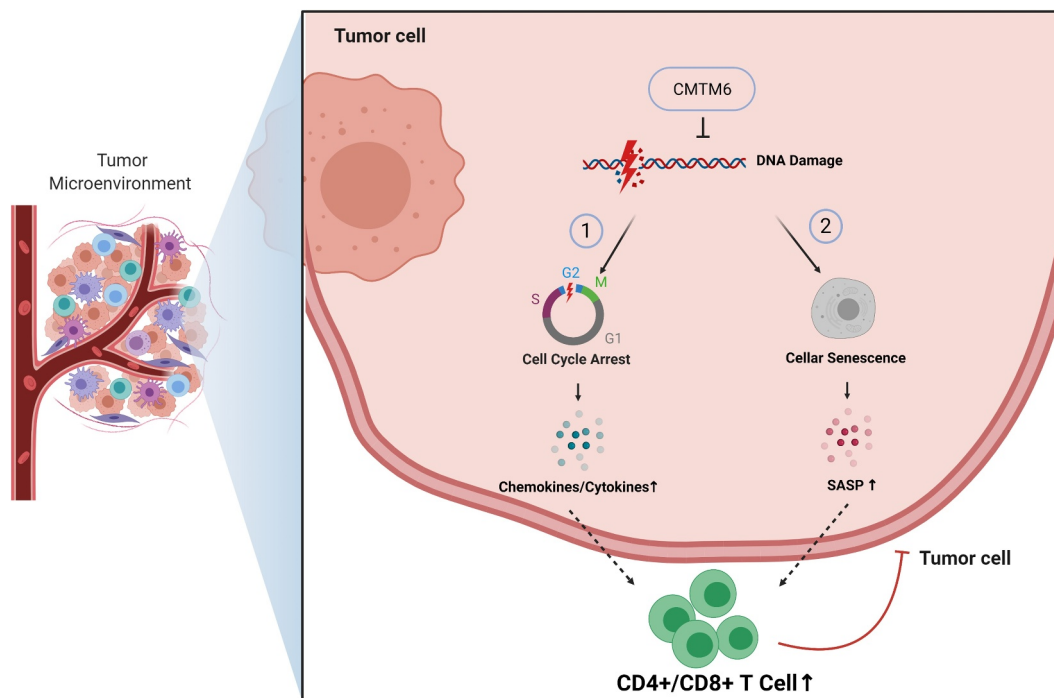
Figure 7. A proposed model for loss of CMTM6 promoting DNA damage-induced cellular senescence and antitumor immunity.

with major malignant characteristics of tumors but also strongly associated with frequent genomic aberrations of driver oncogenes.[12–14] Meanwhile, CMTM6 promotes cell migration and invasion by enhancing EMT progression, a fundamental mechanism for the metastatic phenotype of malignant tumors.[13,30] In our study, we found that CMTM6 was over-expressed in ccRCC tissues and was significantly associated with advanced tumor grade, early lymph node and distant metastases, and adverse prognosis. Interestingly, HKC cells, a commonly used human renal tubular epithelial cell line with characteristics of being immortalized, expressed similar level of CMTM6 in comparison with that in most of ccRCC cell lines (Figure 2a). In spite of maintaining typical genomics and most functional characteristics, potential alterations on morphological heterogeneity, physiological and biomedical features may still exist between primary human renal tubular epithelial cells and HKC cell line.[31,32] Simultaneously, Western blots and IHC staining showed that CMTM6 expression in adjacent normal tissue was mostly lower than that in corresponding ccRCC tissue, while a small portion of adjacent normal tissues present relative higher CMTM6 expression (Figure 1a,b), indicating the CMTM6 expression heterogeneity in ccRCC. In addition, CMTM6 co-localizes with PD-L1 at the plasma membrane and in recycling endosomes, where it prevents PD-L1 from being targeted for lysosome-mediated degradation.[10,11] A positive correlation between the expression of CMTM6 and PD-L1 has been observed,[33–35] and their co-expression has already been identified as a novel prognostic factor in several cancers.[36–38] However, in the current study, we demonstrated for the first time that CMTM6 did not regulate the expression of PD-L1 in ccRCC cells, and no correlation was observed between CMTM6 and PD-L1 expression in ccRCC tissues. This suggests that the biological function of CMTM6 may vary in different types of cancers.

In ccRCC, substantial downregulation of CMTM4 was found, and restoration of CMTM4 significantly suppressed 786-O cell growth by inducing G2/M arrest and p21 upregulation.[39] CMTM6, another member of the CMTM family, shares 55% homology with CMTM4.[11] We showed that CMTM6 expression not only fluctuated following cell cycle progression, peaking in the G2/M phase but also was localized in the nucleus, not just in cellular cytoplasm and membrane. CMTM6 depletion could induce robust DNA damage, resulting in micronucleus formation, an indicator of chromosomal instability and G2/M checkpoint arrest. In addition, CMTM6 expression in pancreatic cancer could be down-regulated by a WEE1 inhibitor, which plays an essential role in the regulation of G2/M checkpoint and DDR.[15] Whether WEE1 is involved in the regulation of CMTM6 and how CMTM6 influences the DDR in ccRCC cells needs to be further investigated. Interestingly, p53 expression concurrently decreased after CMTM6 depletion, which was contradicted the classical "ATM/ATR–CHK1/CHK2–p53" pathway, in which the different activation levels of p53 are dependent on different DNA damage levels.[40] p53 is commonly stabilized by DDR signaling in the presence of DNA damage, but an increasing amount of evidence indicates that there is a more complicated regulatory network than phosphorylation that contributes to p53 stabilization.[41–43] Therefore, the specific mechanisms for DNA damage caused by CMTM6 depletion and the subsequent decrease in p53 need to be studied further. The present study uncovered a novel approach for CMTM6-mediated maintenance of genome stability in ccRCC.

Apart from the activation of cell cycle arrest, DNA damage is also an inducer of cellular senescence. Senescence is a cell fate triggered by stressors or developmental signals and is characterized by stable growth arrest, active metabolism, resistance to cell death, and secretion of extracellular factors.[9] In

this study, we found that CMTM6 depletion in ccRCC cells remarkably transformed the cell morphology and few cells ultimately died. SA-β-Gal staining confirmed that CMTM6 inhibition induced massive cellular senescence. In addition, RNA-seq analysis also revealed that numerous chemokines and cytokines are involved in the top 30 upregulated genes after CMTM6 depletion in ccRCC cells, including many classic markers of SASP such as IL6, CXCL8, CCL2/5, and MMP1/9. SASP commonly acts as a double edged sword in various cancers.[8,9,44] Given the complex array of genes in the SASP and variability of expression in different cell types, these secreted factors can either promote immune surveillance and tumor clearance or create an immunosuppressive, pro-tumor, chemo-resistant environment.[8] For illustration, CCL2 exerted tumor-suppressive responses by recruiting tumor-infiltration cytotoxic T lymphocyte in many solid tumors;[45,46] inversely, CCL2 could also promote breast cancer metastasis by CCL2-induced retention of metastasis-associated macrophages. CXCL8 could not only enhance antitumor immune responses by increasing immunogenicity of dying tumor cells by translocating calreticulin to the cell surface,[47,48] but also promote growth and proliferation of prostate cancer cells through upregulating CXCR7 expression along with ligand-independent function of CXCR7.[49,50] Notably, in the current study, the mRNA level of Ccl2 and Cxcl8 in Renca-shCMTM6 cells was inconsistent with their serum concentrations, which indicated that senescent tumor-derived inflammatory mediators were just an uncertain portion that might do not adequately represent their real final status in local microenvironment or even systemically. However, the results of orthotopic syngeneic graft models indicated T cells are partially responsible for tumor and metastasis control. Overall, SASP in the current study probably contributed to tumor suppression effects that presenting infiltration of CD4$^+$ and CD8$^+$ T cells and decreased the number of CD11b$^+$ MDSC in the syngeneic graft mouse model. Therefore, we speculated that the loss of CMTM6 promote antitumor immunity by inducing senescence and SASP.

Notably, most of the elevated inflammatory cytokines were validated using the results of RNA-seq in our study, few of them, such as CSF2, IL12A, and IL24, were not involved in traditional SASP. Previous studies reported that several inflammatory cytokines could be upregulated, accompanied by G2/M phase arrest, by interfering with exogenous agents.[51,52] Therefore, we presumed that the expression of these inflammatory cytokines was elevated in the G2/M phase. Cell cycle synchronization of ccRCC cells was performed, and we detected their expression patterns in different phases. As expected, most of the inflammatory cytokines were expressed in a cell cycle-dependent manner, fluctuating after cell cycle progression and peaking in G2/M phases. Collectively, the elevated inflammatory cytokines that were found to be involved based on the results of our study were regulated by dual mechanisms.

Although we demonstrated that CMTM6 depletion increases genome instability, leading to following activation of cellular senescence, the underlying mechanisms remains unknown. Dynamic transcriptome profiling of DNA damage-induced cellular senescence predicted that many transcription factors, such as NFYA, PLAU, ATF1, ATF3 and ATF4, may play key roles in regulating DNA repair and senescent cell fates.[53] Correspondingly, RNA-seq analysis in our study revealed that levels of NFY-B, NFY-C (another two subunits of the transcription factor NFY), PLAU, ATF1, ATF4, E2F2, E2F3 and RB1 were dramatically changed, as well as RUNX family and ELF4. NFY is known as a classic transcriptional regulator of cell cycle genes in senescence,[54] ATF4 is involved in DNA repair.[55] In addition, growing evidence implicates RUNX family transcription factors are frequently dysregulated in cancers and function as regulators for DNA damage response.[56] ELF4, a member of the ETS family of transcription factors, contributes to the persistence of γH2A.X DNA damage foci and the absence of ELF4 promotes the faster repair of damaged DNA and more rapid disappearance of γH2A.X foci.[57] Therefore, we suspected that transcription factors might be involved in CMTM6-mediated DNA damage and following activation of cellular senescence, further research to clarify the underlying mechanisms is urgently needed.

In conclusion, this study identified a novel and fundamental role of CMTM6 in the development of ccRCC. CMTM6 depletion promotes DNA damage-induced G2/M checkpoint arrest and cellular senescence with robust inflammatory cytokine secretion, contributing to tumor microenvironment modeling and enhancing anti-tumor immunity (Figure 7). Therefore, targeting CMTM6 may be a promising alternative strategy for ccRCC treatment. Future studies that investigate the specific mechanisms for DNA damage caused by CMTM6 depletion need to be performed.

Author contributions

Xu zhang, Yan Huang and hanfeng Wang conceived the project and designed the experiments. Hanfeng Wang, Yang Fan performed the cell experiments. Hanfeng Wang, Weihao Chen, Zheng Lv, Shengpan Wu conducted the plasmid construction and molecular experiments. Zheng Lv, Chenfeng Wang, Yongliang Lu provided the human tissue samples and clinical information. Hanfeng Wang and Tao Guo performed the immunofluorescence assays. Hanfeng Wang, Shengpan Wu and Donglai Shen performed the IHC and H&E staining. Hanfeng Wang, Weihao Chen, Shengpan Wu and Yongliang Lu performed the animal experiments. Yundong Xuan and Qingbo Huang performed the bioinformatics analyses and conducted the RNA sequencing analysis. Hanfeng Wang, Yan Huang, Fan Zhang and Yu Gao analyzed and interpreted the data. Yan Huang and Xu Zhang supervised the overall execution of the experiments. The manuscript was written by Hanfeng Wang with support from Baojun Wang, Hongzhao Li, Xin Ma, Yan Huang and Xu Zhang. All authors have read and approved the final manuscript.

Disclosure statement

Funding

References

1. Sung H, Ferlay J, Siegel RL, Laversanne M, Soerjomataram I, Jemal A, Bray F. Global cancer statistics 2020: GLOBOCAN estimates of incidence and mortality worldwide for 36 cancers in 185 countries. CA Cancer J Clin. 2021;71(3):209–249. doi:10.3322/caac.21660.

2. Gupta K, Miller JD, Li JZ, Russell MW, Charbonneau C. Epidemiologic and socioeconomic burden of metastatic renal cell carcinoma (mRCC): a literature review. Cancer Treat Rev. 2008;34 (3):193–205. doi:10.1016/j.ctrv.2007.12.001.

3. Jonasch E, Walker CL, Rathmell WK. Clear cell renal cell carcinoma ontogeny and mechanisms of lethality. Nat Rev Nephrol. 2021;17(4):245–261. doi:10.1038/s41581-020-00359-2.

4. Barata PC, Rini BI. Treatment of renal cell carcinoma: current status and future directions. CA Cancer J Clin. 2017;67 (6):507–524. doi:10.3322/caac.21411.

5. Greef B, Eisen T. Medical treatment of renal cancer: new horizons. Br J Cancer. 2016;115(5):505–516. doi:10.1038/bjc.2016.230.

6. Reislander T, Groelly FJ, Tarsounas M. DNA damage and cancer immunotherapy: a STING in the tale. Mol Cell. 2020;80(1):21–28. doi:10.1016/j.molcel.2020.07.026.

7. Rodier F, Coppe JP, Patil CK, Hoeijmakers WA, Munoz DP, Raza SR, Freund A, Campeau E, Davalos AR, Campisi J. Persistent DNA damage signalling triggers senescence-associated inflammatory cytokine secretion. Nat Cell Biol. 2009;11 (8):973–979. doi:10.1038/ncb1909.

8. Rao SG, Jackson JG. SASP: tumor suppressor or promoter? Yes! Trends Cancer. 2016;2(11):676–687. doi:10.1016/j.trecan.2016.10.001.

9. Lopes-Paciencia S, Saint-Germain E, Rowell MC, Ruiz AF, Kalegari P, Ferbeyre G. The senescence-associated secretory phenotype and its regulation. Cytokine. 2019;117:15–22. doi:10.1016/j.cyto.2019.01.013.

10. Burr ML, Sparbier CE, Chan YC, Williamson JC, Woods K, Beavis PA, Lam EYN, Henderson MA, Bell CC, Stolzenburg S, et al. CMTM6 maintains the expression of PD-L1 and regulates anti-tumour immunity. Nature. 2017;549(7670):101–105. doi:10.1038/nature23643.

11. Mezzadra R, Sun C, Jae LT, Gomez-Eerland R, de Vries E, Wu W, Logtenberg MEW, Slagter M, Rozeman EA, Hofland I, et al. Identification of CMTM6 and CMTM4 as PD-L1 protein regulators. Nature. 2017;549(7670):106–110. doi:10.1038/nature23669.

12. Chen L, Yang QC, Li YC, Yang LL, Liu JF, Li H, Xiao Y, Bu -L-L, Zhang W-F, Sun Z-J, et al. Targeting CMTM6 suppresses stem cell-like properties and enhances antitumor immunity in head and neck squamous cell carcinoma. Cancer Immunol Res. 2020;8 (2):179–191. doi:10.1158/2326-6066.CIR-19-0394.

13. Zheng Y, Wang C, Song A, Jiang F, Zhou J, Li G, Zhang W, Ye J, Ding X, Zhang W, et al. CMTM6 promotes cell proliferation and invasion in oral squamous cell carcinoma by interacting with NRP1. Am J Cancer Res. 2020;10(6):1691–1709.

14. Guan X, Zhang C, Zhao J, Sun G, Song Q, Jia W. CMTM6 overexpression is associated with molecular and clinical characteristics of malignancy and predicts poor prognosis in gliomas. EBioMedicine. 2018;35:233–243. doi:10.1016/j.ebiom.2018.08.012.

15. Jin MH, Nam AR, Park JE, Bang JH, Bang YJ, Oh DY. Therapeutic Co-targeting of WEE1 and ATM downregulates PD-L1 expression in pancreatic cancer. Cancer Res Treat. 2020;52(1):149–166. doi:10.4143/crt.2019.183.

16. Gao Y, Li H, Ma X, Fan Y, Ni D, Zhang Y, Huang Q, Liu K, Li X, Wang L, et al. KLF6 suppresses metastasis of clear cell renal cell carcinoma via transcriptional repression of E2F1. Cancer Res. 2017;77(2):330–342. doi:10.1158/0008-5472.CAN-16-0348.

17. Moch H, Cubilla AL, Humphrey PA, Reuter VE, Ulbright TM. The 2016 WHO classification of tumours of the urinary system and male genital organs-part A: renal, penile, and testicular tumours. Eur Urol. 2016;70(1):93–105. doi:10.1016/j.eururo.2016.02.029.

18. Paner GP, Stadler WM, Hansel DE, Montironi R, Lin DW, Amin MB. Updates in the eighth edition of the tumor-node-metastasis staging classification for urologic cancers. Eur Urol. 2018;73(4):560–569. doi:10.1016/j.eururo.2017.12.018.

19. Huang Y, Li W, Yan W, Wu J, Chen L, Yao X, Gu F, Lv L, Zhao J, Zhao M, et al. Loss of PICH promotes chromosome instability and cell death in triple-negative breast cancer. Cell Death Dis. 2019;10 (6):428. doi:10.1038/s41419-019-1662-6.

20. Pan X, Zhou T, Tai YH, Wang C, Zhao J, Cao Y, Chen Y, Zhang P-J, Yu M, Zhen C, et al. Elevated expression of CUEDC2 protein confers endocrine resistance in breast cancer. Nat Med. 2011;17(6):708–714. doi:10.1038/nm.2369.

21. Horikawa N, Abiko K, Matsumura N, Hamanishi J, Baba T, Yamaguchi K, Yoshioka Y, Koshiyama M, Konishi I. Expression of vascular endothelial growth factor in ovarian cancer inhibits tumor immunity through the accumulation of myeloid-derived suppressor cells. Clin Cancer Res. 2017;23(2):587–599. doi:10.1158/1078-0432.CCR-16-0387.

22. Livak KJ, Schmittgen TD. Analysis of relative gene expression data using real-time quantitative PCR and the 2−ΔΔCT method. Methods. 2001;25(4):402–408. doi:10.1006/meth.2001.1262.

23. Ma HT, Poon RY. Synchronization of HeLa cells. Methods Mol Biol. 2017;1524:189–201.

24. Zhang J, Bu X, Wang H, Zhu Y, Geng Y, Nihira NT, Tan Y, Ci Y, Wu F, Dai X. Cyclin D-CDK4 kinase destabilizes PD-L1 via cullin 3-SPOP to control cancer immune surveillance. Nature. 2018;553 (7686):91–95. doi:10.1038/nature25015.

25. Lanz MC, Dibitetto D, Smolka MB. DNA damage kinase signaling: checkpoint and repair at 30 years. EMBO J. 2019;38(18):e101801. doi:10.15252/embj.2019101801.

26. Wang Y, Luo M, Chen Y, Wang Y, Zhang B, Ren Z, Bao L, Wang Y, Wang JE, Fu Y-X, et al. ZMYND8 expression in breast cancer cells blocks T-Lymphocyte surveillance to promote tumor growth. Cancer Res. 2021;81(1):174–186. doi:10.1158/0008-5472.CAN-20-1710.

27. Bartkova J, Rezaei N, Liontos M, Karakaidos P, Kletsas D, Issaeva N, Vassiliou LVF, Kolettas E, Niforou K, Zoumpourlis VC, et al. Oncogene-induced senescence is part of the tumorigenesis barrier imposed by DNA damage checkpoints. Nature. 2006;444(7119):633–637. doi:10.1038/nature05268.

28. Di Micco R, Fumagalli M, Cicalese A, Piccinin S, Gasparini P, Luise C, Schurra C, Garre' M, Giovanni Nuciforo P, Bensimon A, et al. Oncogene-induced senescence is a DNA damage response triggered by DNA hyper-replication. Nature. 2006;444 (7119):638–642. doi:10.1038/nature05327.

29. Zhao Y, Zhang M, Pu H, Guo S, Zhang S, Wang Y. Prognostic implications of pan-cancer CMTM6 expression and its relationship with the immune microenvironment. Front Oncol. 2020;10:585961. doi:10.3389/fonc.2020.585961.

30. Huang X, Xiang L, Wang B, Hu J, Liu C, Ren A, Du K, Ye G, Liang Y, Tang Y, et al. CMTM6 promotes migration, invasion, and EMT by interacting with and stabilizing vimentin in hepatocellular carcinoma cells. J Transl Med. 2021;19(1):120. doi:10.1186/s12967-021-02787-5.

31. Ebert T, Bander NH, Finstad CL, Ramsawak RD, Old LJ. Establishment and characterization of human renal cancer and normal kidney cell lines. Cancer Res. 1990;50:5531–5536.

32. Ryan MJ, Johnson G, Kirk J, Fuerstenberg SM, Zager RA, Torok-Storb B. HK-2: an immortalized proximal tubule epithelial cell line from normal adult human kidney. Kidney Int. 1994;45(1):48–57. doi:10.1038/ki.1994.6.

33. Shang X, Li J, Wang H, Li Z, Lin J, Chen D, Wang H. CMTM6 is positively correlated with PD-L1 expression and immune cells infiltration in lung squamous carcinoma. Int Immunopharmacol. 2020;88:106864. doi:10.1016/j.intimp.2020.106864.

34. Li X, Chen L, Gu C, Sun Q, Li J. CMTM6 significantly relates to PD-L1 and predicts the prognosis of gastric cancer patients. PeerJ. 2020;8:e9536. doi:10.7717/peerj.9536.

35. Wang H, Gao J, Zhang R, Li M, Peng Z, Wang H. Molecular and immune characteristics for lung adenocarcinoma patients with CMTM6 overexpression. Int Immunopharmacol. 2020;83:106478. doi:10.1016/j.intimp.2020.106478.

36. Liu LL, Zhang SW, Chao X, Wang CH, Yang X, Zhang XK, Wen Y-L, Yun J-P, Luo R-Z. Coexpression of CMTM6 and PD-L1 as a predictor of poor prognosis in macrotrabecular-massive hepatocellular carcinoma. Cancer Immunol Immunother. 2021;70 (2):417–429. doi:10.1007/s00262-020-02691-9.

37. Zhang C, Zhao S, Wang X. Co-expression of CMTM6 and PD-L1: a novel prognostic indicator of gastric cancer. Cancer Cell Int. 2021;21(1):78. doi:10.1186/s12935-020-01734-6.

38. Peng QH, Wang CH, Chen HM, Zhang RX, Pan ZZ, Lu ZH, Wang G-Y, Yue X, Huang W, Liu R-Y. CMTM6 and PD-L1 coexpression is associated with an active immune microenvironment and a favorable prognosis in colorectal cancer. J Immunother Cancer. 2021;9(2):e001638. doi:10.1136/jitc-2020-001638.

39. Li T, Cheng Y, Wang P, Wang W, Hu F, Mo X, Lv H, Xu T, Han W. CMTM4 is frequently downregulated and functions as a tumour suppressor in clear cell renal cell carcinoma. J Exp Clin Cancer Res. 2015;34(1):122. doi:10.1186/s13046-015-0236-4.

40. Roos WP, Thomas AD, Kaina B. DNA damage and the balance between survival and death in cancer biology. Nat Rev Cancer. 2016;16(1):20–33. doi:10.1038/nrc.2015.2.

41. Ashcroft M, Kubbutat MH, Vousden KH. Regulation of p53 function and stability by phosphorylation. Mol Cell Biol. 1999;19 (3):1751–1758. doi:10.1128/MCB.19.3.1751.

42. Blattner C, Tobiasch E, Litfen M, Rahmsdorf HJ, Herrlich P. DNA damage induced p53 stabilization: no indication for an involvement of p53 phosphorylation. Oncogene. 1999;18(9):1723–1732. doi:10.1038/sj.onc.1202480.

43. Leng RP, Lin Y, Ma W, Wu H, Lemmers B, Chung S, Parant JM, Lozano G, Hakem R, Benchimol S. Pirh2, a p53-induced ubiquitin-protein ligase, promotes p53 degradation. Cell. 2003;112(6):779–791. doi:10.1016/S0092-8674(03)00193-4.

44. Liu XL, Ding J, Meng LH. Oncogene-induced senescence: a double edged sword in cancer. Acta Pharmacol Sin. 2018;39 (10):1553–1558. doi:10.1038/aps.2017.198.

45. Lanca T, Costa MF, Goncalves-Sousa N, Rei M, Grosso AR, Penido C, Silva-Santos B. Protective role of the inflammatory CCR2/CCL2 chemokine pathway through recruitment of type 1 cytotoxic γδ T lymphocytes to tumor beds. J Immunol. 2013;190 (12):6673–6680. doi:10.4049/jimmunol.1300434.

46. Berencsi K, Rani P, Zhang T, Gross L, Mastrangelo M, Meropol NJ, Herlyn D, Somasundaram R. In vitro migration of cytotoxic T lymphocyte derived from a colon carcinoma patient is dependent on CCL2 and CCR2. J Transl Med. 2011;9(1):33. doi:10.1186/1479-5876-9-33.

47. Nagarsheth N, Wicha MS, Zou W. Chemokines in the cancer microenvironment and their relevance in cancer immunotherapy. Nat Rev Immunol. 2017;17(9):559–572. doi:10.1038/nri.2017.49.

48. Sukkurwala AQ, Martins I, Wang Y, Schlemmer F, Ruckenstuhl C, Durchschlag M, Michaud M, Senovilla L, Sistigu A, Ma Y. Immunogenic calreticulin exposure occurs through a phylogenetically conserved stress pathway involving the chemokine CXCL8. Cell Death Differ. 2014;21(1):59–68. doi:10.1038/cdd.2013.73.

49. Caruso DJ, Carmack AJ, Lokeshwar VB, Duncan RC, Soloway MS, Lokeshwar BL. Osteopontin and interleukin-8 expression is independently associated with prostate cancer recurrence. Clin Cancer Res. 2008;14(13):4111–4118. doi:10.1158/1078-0432.CCR-08-0738.

50. Liu Q, Li A, Tian Y, Wu JD, Liu Y, Li T, Chen Y, Han X, Wu K. The CXCL8-CXCR1/2 pathways in cancer. Cytokine Growth Factor Rev. 2016;31:61–71. doi:10.1016/j.cytogfr.2016.08.002.

51. Wang W, Yu X, Wu C, Jin H. Differential effects of Wnt5a on the proliferation, differentiation and inflammatory response of keratinocytes. Mol Med Rep. 2018;17(3):4043–4048. doi:10.3892/mmr.2017.8358.

52. Zhang L, Hao Q, Bao L, Liu W, Fu X, Chen Y, Wu H. Phenethyl isothiocyanate suppresses cervical carcinoma metastasis potential and its molecular mechanism. Mol Med Rep. 2014;10 (5):2675–2680. doi:10.3892/mmr.2014.2565.

53. Zhao Z, Dong Q, Liu X, Wei L, Liu L, Li Y, Wang X. Dynamic transcriptome profiling in DNA damage-induced cellular senescence and transient cell-cycle arrest. Genomics. 2020;112 (2):1309–1317. doi:10.1016/j.ygeno.2019.07.020.

54. Matuoka K, Yu Chen K. Nuclear factor Y (NF-Y) and cellular senescence. Exp Cell Res. 1999;253(2):365–371. doi:10.1006/excr.1999.4605.

55. Fung H, Liu P, Demple B. ATF4-dependent oxidative induction of the DNA repair enzyme Ape1 counteracts arsenite cytotoxicity and suppresses arsenite-mediated mutagenesis. Mol Cell Biol. 2007;27 (24):8834–8847. doi:10.1128/MCB.00974-07.

56. Samarakkody AS, Shin NY, Cantor AB. Role of RUNX family transcription factors in DNA damage response. Mol Cells. 2020;43(2):99–106. doi:10.14348/molcells.2019.0304.

57. Sashida G, Bae N, Di Giandomenico S, Asai T, Gurvich N, Bazzoli E, Liu Y, Huang G, Zhao X, Menendez S. The mef/elf4 transcription factor fine tunes the DNA damage response. Cancer Res. 2011;71(14):4857–4865. doi:10.1158/0008-5472.CAN-11-0455.